

Metal-Functionalized Hydrogels as Efficient Oxygen Evolution Electrocatalysts

Chaoyun Tang, Belvin Thomas, Maricely Ramírez-Hernández, Eliška M. Mikmeková, and Tewodros Asefa*



Cite This: <https://doi.org/10.1021/acsami.2c01667>



Read Online

ACCESS |



Metrics & More



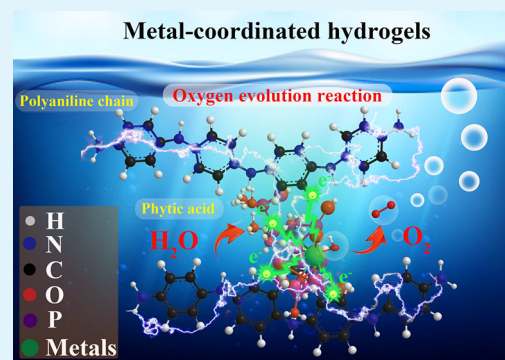
Article Recommendations



Supporting Information

ABSTRACT: Conductive polymer hydrogels have large surface areas and electrical conductivities. Their properties can be further tailored by functionalizing them with metals and nonmetals. However, the potential applications of metal-functionalized hydrogels for electrocatalysis have rarely been investigated. In this work, we report the synthesis of transition-metal-functionalized polyaniline–phytic acid (PANI–PA) hydrogels that show efficient electrocatalytic activities for the oxygen evolution reaction (OER). Among the many transition metals studied, Fe is accommodated by the hydrogel the most due to the favorable affinity of the PA groups in the hydrogel for Fe. Meanwhile, those containing both Fe and Co are found to be the most effective electrocatalysts for OER. The most optimized such hydrogel, NF@Hgel-Fe_{0.3}Co_{0.1}, which is made using a solution that has a 3:1 ratio of Fe and Co, needs an overpotential of only 280 mV to catalyze OER in 1 M KOH solution with a current density of 10 mV cm⁻². Furthermore, these metal-functionalized PANI–PA hydrogels can easily be loaded on the nickel foam or carbon cloth via a simple soak-and-dry method to generate free-standing electrodes. Overall, this work demonstrates a facile synthesis and fabrication of sustainable and efficient OER electrocatalysts and electrodes that are composed of easily processable hydrogels functionalized with earth-abundant transition metals.

KEYWORDS: hydrogel, conducting polymer, oxygen evolution reaction, phytic acid, polyaniline



1. INTRODUCTION

The growing energy crisis and environmental pollution caused by our over-reliance on fossil fuels have stimulated great interest in developing various alternative energy conversion and storage technologies, such as water electrolyzers, fuel cells, and metal–air batteries.^{1,2} Water electrolyzers produce green hydrogen from water through the hydrogen evolution reaction, in conjunction with the oxygen evolution reaction (OER). Of these two half-reactions, the OER is more difficult to carry out because it involves several energy-intensive reaction steps. This makes the overall OER kinetics very sluggish and require a large overpotential.³ As a result, catalysts that can speed up the reaction steps in OER are needed to efficiently split water into H₂ and O₂. Besides, the catalysts must be stable and composed of readily available elements to be cost-effective and scalable for practical use.

Up until now, the state-of-the-art electrocatalysts for OER are Ru- and Ir-based materials. However, the scarcity and high cost of Ru and Ir render these catalysts impractical for widespread use.⁴ A great deal of effort and progress has already been made toward the development of alternative OER electrocatalysts with earth-abundant elements, including carbon nanomaterials and transition-metal oxides, hydroxides, oxyhydroxides, and phosphates.⁵ However, although many of them show good

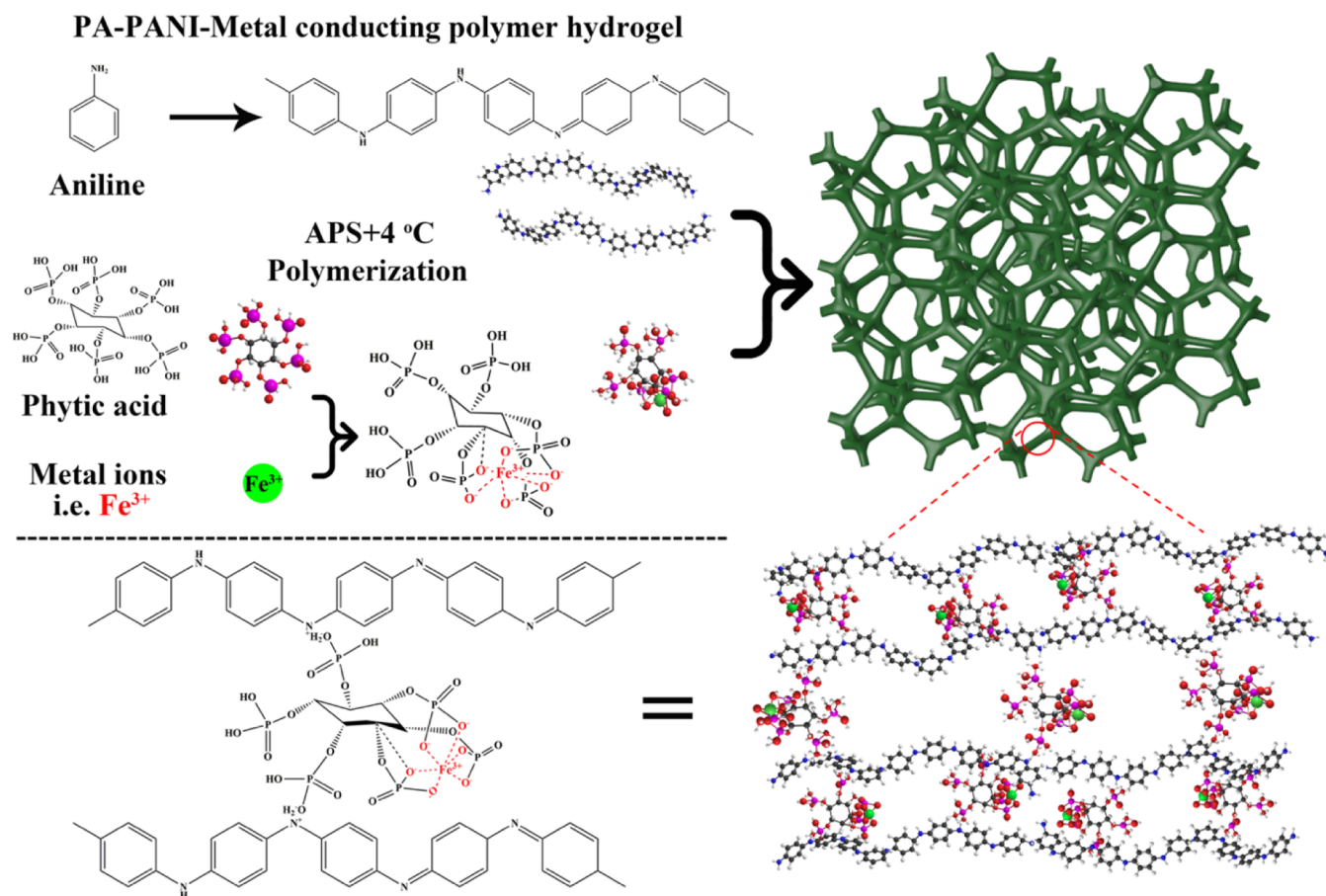
electrocatalytic activities for OER, they still fail to replace noble metal-based catalysts, especially for industrial scale applications.

Polymer hydrogels composed of conjugated polymers, such as polyaniline (PANI) and polypyrrole, possess three-dimensional microstructures and high hydrability (which means a strong interaction with water). Moreover, they can easily be synthesized from their monomers using simple polymerization reactions. These hydrogels also have high conductivity, strong structural stability, and great ability to form good interfaces with electron-transporting phases (electrodes) and ion-transporting phases (electrolytes). Therefore, they are attractive for various electrochemical applications, including electrocatalysis.⁶

In 2012, Pan et al.⁷ reported a polymer hydrogel composed of PANI and phytic acid (PA) that showed a record conductivity of 0.11 S·cm⁻¹. The authors also demonstrated that the hydrogel could easily be processed with ink-jet printing or spray-coating

Received: January 26, 2022

Accepted: April 18, 2022

Scheme 1. Schematic Illustration of the Synthesis of PANI–PA–Metal (Hgel-M_x) Hydrogels for Electrocatalysis of OER^a

^aWhile the scheme specifically illustrates for Fe³⁺ ions, the method equally applies to other transition-metal ions (see also Figure S1 in the Supporting Information).

into various micropatterns for applications in supercapacitors and sensors. In 2019, Hu et al. reported that polypyrrole–PA hydrogels could electrocatalyze OER.⁸ Some of these polymers could also be transformed into other types of electrocatalysts through an additional synthetic step. For example, Zhang et al. reported that the pyrolysis of PANI hydrogels at 1000 °C would lead to three-dimensional mesoporous carbon foams that exhibit electrocatalytic activities for both OER and ORR.⁹ However, the electrocatalytic performances of the polymer hydrogels reported so far are too low to be viable for practical applications.⁴ Therefore, various additional approaches (e.g., introduction of non-noble metals, as demonstrated herein) to synthesize hydrogels with improved electrocatalytic performances should be explored.

PA is a major inorganic phosphate ester, which plant seeds use to store phosphorus with.¹⁰ Coupling PA with conducting polymers, such as PANI, is reported to lead to hydrogels as well as to tailor the structural and electronic properties of these polymers.^{7,8} Moreover, PA has an ability to chelate metal ions such as Fe³⁺, Zn²⁺, Ca²⁺, and Mn²⁺.¹¹ Thus, by taking advantage of its ability to coordinate metals, the PA groups infiltrated into polymers, such as PANI, should help introduce large amounts of metals into these polymers. While this could be an attractive strategy to develop metal-coordinated electroactive conducting polymer hydrogels, the potential applications of such materials for electrocatalysis have been rarely investigated.¹²

In this work, we report a facile synthesis of PANI–PA hydrogels functionalized with various transition metals and their high electrocatalytic activity for OER (Scheme 1). The hydrogels also remain stable and maintain their catalytic activity during the reaction for hours. Among different such hydrogels we have investigated, the one synthesized from a solution containing Fe and Co in a ratio of 3:1 is found to be the most effective electrocatalyst for OER, requiring an overpotential of 280 mV to drive the reaction at a current density of 10 mA cm^{−2} in an alkaline solution. To the best of our knowledge, this is the first report where PA-modified PANI hydrogels that are functionalized with transition-metal ions are synthesized and then demonstrated to efficiently electrocatalyze OER. Thus, the work could provide an impetus for the synthesis of other conducting polymer hydrogels containing various non-noble metal ions for electrocatalysis.

2. EXPERIMENTS AND CHARACTERIZATIONS

2.1. Chemicals and Reagents. All chemical and reagents used for the experiments were purchased from Sigma-Aldrich, and they were used as received and without further purification.

2.2. Synthesis of Hydrogels. First, pristine PANI hydrogel was synthesized via a one-step, template-free synthetic process as previously described elsewhere.¹ This hydrogel was used as a reference material for our studies. Then, various metal-functionalized PANI–PA hydrogels were synthesized, as illustrated in Scheme 1 above and in Figure S1 in the Supporting Information. In a typical synthesis, 0.4 mmol of metal nitrate, namely, iron(III) nitrate nonahydrate (Fe(NO₃)₃·9H₂O),

iron(II) chloride (FeCl_2), iron(II) sulfate (FeSO_4), cobalt(II) nitrate hexahydrate ($\text{Co}(\text{NO}_3)_2 \cdot 6\text{H}_2\text{O}$), nickel(II) nitrate hexahydrate ($\text{Ni}(\text{NO}_3)_2 \cdot 6\text{H}_2\text{O}$), zinc(II) nitrate hexahydrate ($\text{Zn}(\text{NO}_3)_2 \cdot 6\text{H}_2\text{O}$), copper(II) nitrate hexahydrate ($\text{Cu}(\text{NO}_3)_2 \cdot 6\text{H}_2\text{O}$), or manganese(II) nitrate hexahydrate ($\text{Mn}(\text{NO}_3)_2 \cdot 6\text{H}_2\text{O}$), was dissolved in deionized (DI) water (2 mL) and HCl (4 mL, 1 M). Into the solution, aniline (i.e., the monomer of PANI) (0.5 mL) and PA solution (1 mL, 50% wt/wt in water) were added. After ultrasonication for 30 min, a homogenous solution, named "Solution A," was obtained. Separately, ammonium persulfate (0.286 g or 1.25 mmol) was dissolved in deionized (DI) water (1 mL) to obtain a solution named "Solution B". After pouring Solution B into Solution A, the mixture was cooled to $\sim 4^\circ\text{C}$ immediately. After keeping the mixture under static conditions for 24 h, the polymerization of aniline took place, and a hydrogel was obtained. The hydrogel was washed with DI water five times to remove any residual acid or reaction byproducts. It was then dried in an oven at 80°C . The resulting as-synthesized hydrogels were denoted as Hgel- M_x , where M represents Fe, Co, Ni, Zn, Cu, or Mn, and x stands for the amount (of metal) in millimole. To prepare hydrogels cofunctionalized with two different metals, solutions containing two metal salts in different ratios were used under an otherwise similar procedure. As an additional reference material, a hydrogel containing no metals (Hgel) was prepared in the same way but without including metal salts in the solution.

2.3. Materials Characterizations. Powder X-ray diffraction (XRD) patterns of the materials were recorded using a Bruker X-ray diffractometer (D8 ADVANCE) operating with a $\text{Cu K}\alpha$ X-ray source ($\lambda = 0.154\text{ nm}$). Thermogravimetric analyses of the materials were conducted with a TGA7 instrument (PerkinElmer) at a heating rate of $10^\circ\text{C min}^{-1}$ and under a flow of air at a rate of 20 mL min^{-1} . The exact amounts of metals in the materials were determined with inductively coupled plasma optical emission spectroscopy (ICP-OES) using a 720-ES instrument (Agilent). Raman spectroscopy was conducted using a DXR2xi Raman imaging microscope (Thermo Scientific) that was operating with an excitation wavelength of 633 nm. Fourier transform infrared (FTIR) spectra were recorded using a Nicolet iS 10 FTIR spectrometer (Thermo Scientific). To determine the morphologies, structures, and elemental compositions of the materials, a field-emission scanning electron microscope (Zeiss Supra 55) equipped with energy-dispersive X-ray spectroscopy (EDS) was used. Further morphological and microstructural analyses of the materials were performed using a JEM-2100f high-resolution transmission electron microscope (JEOL). Using the same microscope, selected-area electron diffraction patterns were acquired to study the crystal structure of the materials. The porosity of the materials was determined from N_2 adsorption-desorption measurements at 77 K using a Tristar-3000 porosimeter (Micromeritics). The surface chemical compositions of the materials were analyzed with a K-Alpha X-ray photoemission spectrometer (Thermo Scientific) that was operating with an $\text{Al K}\alpha$ X-ray source ($h\nu = 1486.6\text{ eV}$). To obtain the survey spectra, the scans were carried out in an interval of 1 eV. To obtain high-resolution spectra of individual peaks, the scans were performed in an interval of 0.1 eV. All the binding energies in the X-ray photoelectron spectroscopy (XPS) spectra were calibrated using the C 1s peak (at a binding energy of 284.6 eV) of adventitious hydrocarbons present on the materials.

2.4. Electrochemical Measurements and Electrocatalytic Tests. All electrochemical measurements and electrocatalytic tests were conducted under an ambient environment using an electrochemical setup comprising a VersaSTAT 3 potentiostat/galvanostat (Princeton Applied Research) and the VersaStudio software. In the electrochemical cell, nickel foams (NFs, each with a working area of 1 cm^2) that were loaded with different hydrogels were used as working electrodes, a carbon rod was used as a counter electrode, and a saturated calomel electrode (SCE) was used as a reference electrode. In all measurements, the SCE reference electrode was calibrated with a reversible hydrogen electrode (RHE), and all potentials were recorded with respect to RHE. As an electrolyte, a solution of 1 M KOH was used. The conversion from $E(\text{RHE})$ to $E(\text{SCE})$ was carried out using the equation: $E(\text{RHE}) = E(\text{SCE}) + 0.245\text{ V} + 0.0591\text{ pH}$, where

$E(\text{RHE})$ and $E(\text{SCE})$ represent the potentials of the electrode with respect to RHE and SCE, respectively.

To prepare the working electrodes, typically, 10 mg of the as-prepared hydrogel was dispersed in 10 mL solution of DI water and ethanol with a volume ratio of 4:1 via ultrasonication for 30 min. NF (whose overall size is $1\text{ cm} \times 1.5\text{ cm}$ and whose active area is $1\text{ cm} \times 1\text{ cm}$) was pre-treated in a HCl solution (2 M, 10 mL) for 30 min and washed with DI water. Then, it was immersed into the solution containing the hydrogel and, subsequently, taken out and dried in an oven at 80°C . This procedure was repeated several times until the catalyst loading reached 1 mg cm^{-2} , which was measured as precisely as possible with an analytical balance.

Before each test of OER, five cyclic voltammetry (CV) scans in the range of 1.1–1.9 V versus RHE were performed to activate the as-synthesized electrocatalyst on the electrode. After this, linear sweep voltammetry (LSV) profiles were recorded at a scan rate of 2 mV s^{-1} in a potential window of 1.1 to 1.8 V versus RHE. The data obtained from the measurements were all corrected for iR losses and background currents. Electrochemical impedance spectroscopy (EIS) was performed using a voltage amplitude of 5 mV and different frequencies in the range of 100 kHz to 10 Hz. To determine the electrochemical capacitance of each material, the potential was scanned three times in the non-Faradaic region from 1.1 to 1.2 V versus RHE and using seven different scan rates, namely, 20, 40, 60, 80, 100, 120, and 140 mV s^{-1} . The stability of the electrocatalysts was evaluated with chronoamperometry at overpotentials of 280 and 300 mV for 24 h.

3. RESULTS AND DISCUSSION

3.1. Synthesis and Characterization of Hydrogels and Control Materials. Different PANI–PA hydrogels functionalized with metal ions are synthesized through a procedure involving the polymerization of aniline (to PANI), supramolecular cross-linking of PANI and PA, and adsorption of metal ions into the cross-linked PANI–PA polymer, as illustrated in Scheme 1. As aniline undergoes polymerization in aqueous solution containing PA, the process ultimately forms a hydrogel composed of PANI–PA chains. In the hydrogel, the PA groups end up not only as dopants but also as cross-linkers of PANI chains via electrostatic and hydrogen bonding interactions. When metallic ions, for example, Fe^{3+} ions, coexist in the reaction mixture, they form coordination bonds with PA's phosphate groups resulting in metal-functionalized PANI–PA hydrogels. Residual ions and oligomers are removed from the polymer hydrogels by thoroughly washing the products with deionized (DI) water and then ethanol. Finally, PANI–PA–metal hydrogels, which are also called Hgel-Metal or Hgel- M_x , where M represents Fe, Co, Ni, Zn, Cu, or Mn, and x stands for the amount (of metal) in mmol, are obtained. For comparative studies, pristine hydrogel (Hgel-Norm) is synthesized in the same way but without including metals in the reaction mixture. More synthetic detail is provided in the Experiments and Characterizations section and in Figure S1 in the Supporting Information.

The XRD patterns of all metal-functionalized hydrogels and pristine hydrogel show no noticeable differences among one another (Figure S2a). More specifically, they all show only a broad peak at 2θ of ca. 26° and a shoulder peak at 2θ of ca. 20° . These broad peaks, which are due to the scattering from the periodicity perpendicular and parallel to PANI chains, respectively, are indicative of predominantly amorphous PANI-based materials.^{13–16} Moreover, the XRD patterns show no peaks associated with crystalline metallic species. These results indicate that metal-functionalized PANI–PA hydrogels have similar underlying polymeric structures to the pristine hydrogel.

Thermogravimetric analysis (TGA) performed in an air atmosphere (Figure S3) shows that, except for Fe-functionalized PANI–PA hydrogels, all other metal-functionalized hydrogels as well as the pristine PANI–PA hydrogel have similar TGA curves and give similar amounts of residues at 800 °C (Figure S3a). Interestingly, Fe-functionalized hydrogels produce much more residues (e.g., while the residues at 800 °C of pristine hydrogel, Hgel-Co_{0.4}, and Hgel-Ni_{0.4} are all only ca. 2.38 wt %, that of Hgel-Fe_{0.4} at 800 °C is a whopping 37.08 wt %). This means, among the transition metals investigated, Fe is incorporated into the hydrogel to a much greater extent. Conversely, PANI–PA hydrogel accommodates Fe much more than the other metals.

Additionally, hydrogels containing Fe in different valence states (+2 and +3), along with different counter anions, are synthesized in the same way and then analyzed using TGA. Their TGA curves (Figure S3b) show that both Fe²⁺ and Fe³⁺ ions can be equally incorporated into the PANI–PA hydrogel, and their counter anions, which include NO₃[−], Cl[−], and SO₄^{2−}, barely make a difference. Hydrogels with different amounts of Fe are also synthesized and investigated (Figure S4a,b). As can be expected, the weight of the residues of the hydrogels at 800 °C increases as the amount of Fe used during their synthesis increases. This is true even if a second metal is included in the synthesis of the hydrogels, again indicating the hydrogel's preference to Fe over the other metals. The increase in weight of the residues is linearly related with the amount of Fe included during the synthesis of the hydrogels (Figures S4 and S5). The hydrogel's capacity for Fe starts to wane only when the concentration of Fe³⁺ ions in the reaction mixture is near 0.6 mM.

The amounts of metals in the metal-functionalized hydrogels are determined with ICP-OES. Based on the results, compiled in Tables S1 and S2, the amounts of Fe in the hydrogels are much lower than the weights of their residues at 800 °C observed on their TGA curves. The additional weight in the residues must be due to the formation of iron oxides and carbon. The latter is not unprecedented given the fact that Fe promotes the degree of polymerization of polymers, such as PANI, and the higher degree of carbonization of such conjugated polymers at high temperatures.^{17–19} Nevertheless, the results show that the materials possess a much larger amount of Fe than Co even in cases where a lower amount of Fe than Co is used during the synthesis of the hydrogels.

Raman spectra of all hydrogels (Figure S6) show bands at 1340 and 1566 cm^{−1}, which are due to the stretching vibrations of C–N and C=C bonds in the quinoid/benzenoid rings of PANI, respectively.^{20–22} These bands are weaker in the Raman spectra of Fe-functionalized hydrogels, suggesting that the Fe incorporated into the polymer reduces the breathing vibrations of C–N and C=C bonds in PANI. The FTIR spectra of Hgel-Fe_{0.4} hydrogel and pristine PANI hydrogel show similar bands (Figure 1). These results indicate that, despite the presence of Fe in it, Hgel-Fe_{0.4} possesses an emeraldine structure just like PANI, rather than only the leucoemeraldine or permigraniline structure. The peaks at ca. 1480 and 1569 cm^{−1} in the FTIR spectra are characteristic of the stretching vibrations of quinoid and benzenoid rings of PANI chains, respectively. The bands at 1246 and 1300 cm^{−1} can be assigned to the C–N stretching vibration in the conjugated aromatic rings in the hydrogel. It is generally accepted that the absorption band near 1140 cm^{−1} is due to the N=Q=N stretching mode, where Q denotes a quinoid ring.²³ This band is also indicative of the delocalization of electrons in PANI.¹⁴ The bands at ca. 505 and 796 cm^{−1} are

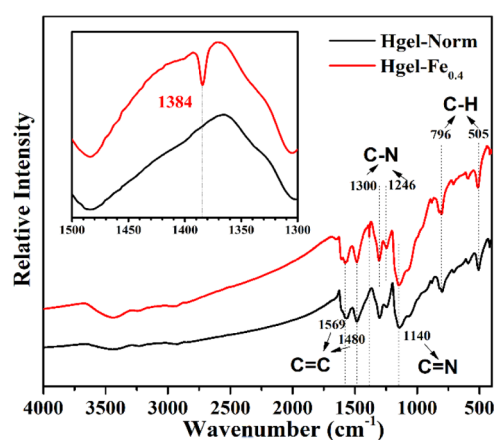


Figure 1. FTIR spectra of pristine hydrogel (or Hgel-Norm) and Hgel-Fe_{0.4} hydrogel. The inset shows the peaks of interest in the spectra that are due to metal–polymer coordination bonds.

attributable to the bending vibrations of the C–H bonds of 1,4-disubstituted aromatic rings present in the PANI–PA polymer. The absorption bands between 3000 and 3500 cm^{−1} are due to the O–H and C–H stretching modes of these groups, which are present in the polymer. The peak at ca. 1384 cm^{−1}, which is observed in the spectra of all metal-functionalized PANI–PA hydrogels (Figures S7 and S8), is due to O=P–O–M species (where M represents Fe, Co, or Ni). This peak is also observed on the FT-IR spectrum of the precipitate formed from the reaction between PA and Fe³⁺ ions in a control experiment, as shown in Figure S9. The UV–vis absorption spectra of all metal-functionalized hydrogels are also like that of the pristine hydrogel (Figure S10), further corroborating their largely similar underlying chemical structures.

Field emission scanning electron microscopy (FESEM) and transmission electron microscopy (TEM) images are obtained to study the structures and morphology of the hydrogels. Pristine hydrogel shows coral-like dendritic/branched nanofibers with visible macropores and micropores on the nanofibers (Figure S11a–f). When Fe is included, not only is the micromorphology of the hydrogel distinctly altered but also its nanofibers transform into closely packed and interconnected nanospheres that however still contain macropores and micropores (Figure S12a–f). As the amount of Fe used to make the hydrogels is increased, the sizes of the nanospheres decrease slightly (Figure S13). However, the addition of Co does not alter the micromorphology of the hydrogel (Figure S14a–f). This must be because the hydrogel takes up much less amount of Co (compared with Fe), and the Co-functionalized hydrogel is thus almost like the pristine hydrogel. Not surprisingly, the FESEM and TEM images of Fe and Co cofunctionalized hydrogel Hgel-Fe_{0.3}Co_{0.1} (Figure 2) are like those of Fe-functionalized hydrogel (Hgel-Fe_{0.4}), indicating once again that Co does not play as much a role as Fe in dictating the micromorphology of the hydrogel.

Elemental mapping images of the hydrogels obtained with EDS (Figures 2g, S11g, S12g and S14g) show well-distributed C, N, O, P, and Fe/Co atoms. The images also reveal the successful incorporation of Fe and Co in the Fe- and Co-cofunctionalized hydrogels. It is worth noting that conductive materials possessing such transition metals together often exhibit better electrocatalytic activity for various reactions compared with those containing only one of them.^{24,25} This is also found to be the case in this work (vide infra). Not surprisingly, the metals are

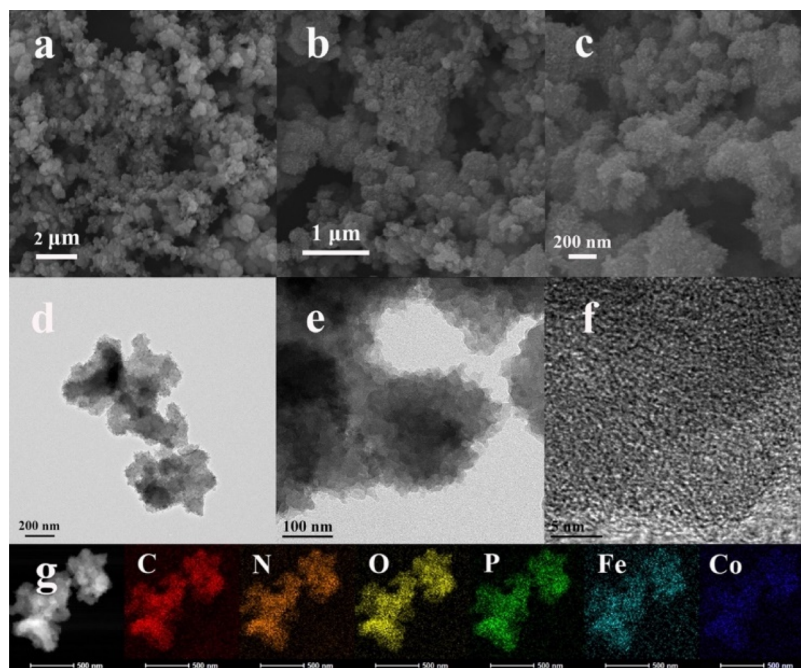


Figure 2. (a–c) FESEM images, (d–f) TEM images in low and high resolutions, and (g) EDS elemental mapping images (showing C, N, O, P, Fe, and Co) of Hgel-Fe_{0.3}Co_{0.1} hydrogels.

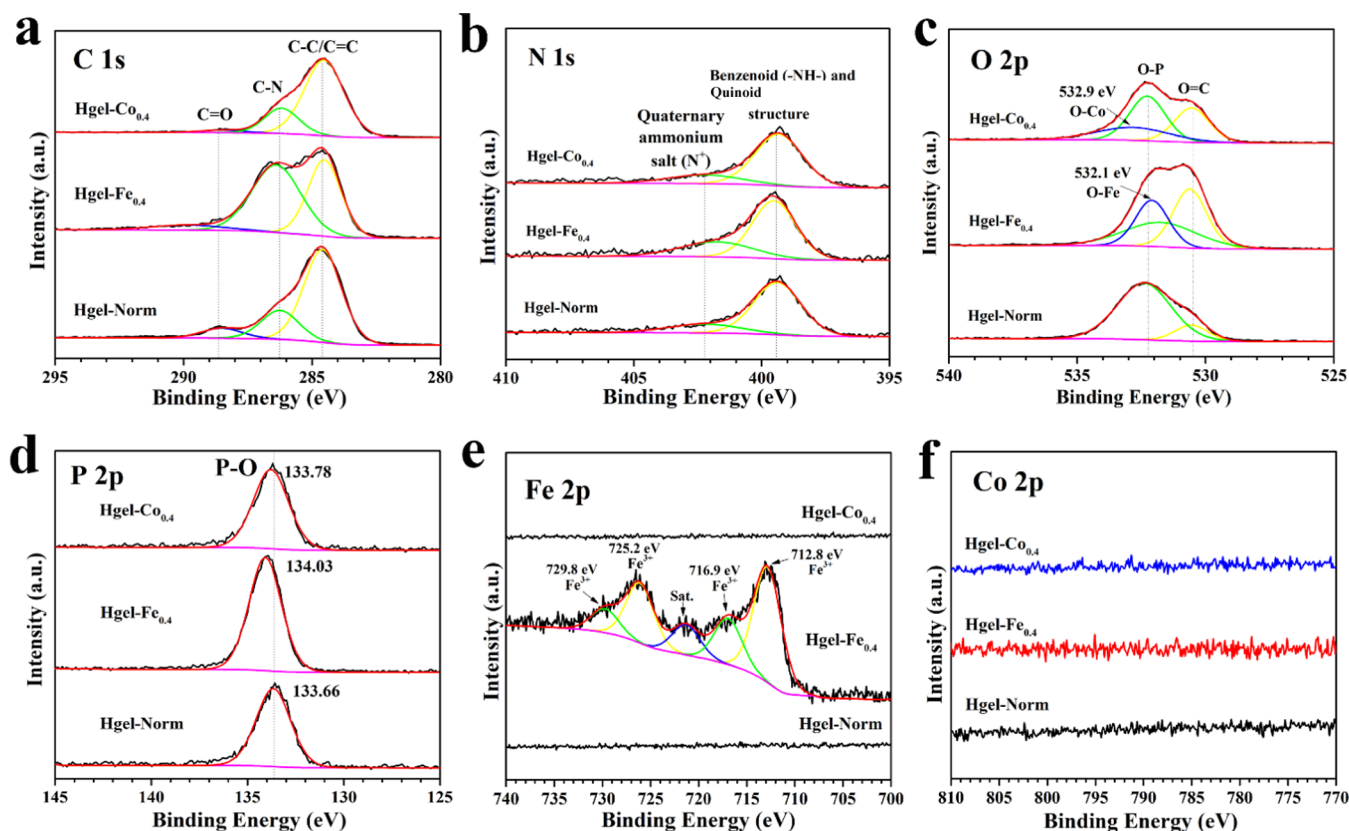


Figure 3. High-resolution XPS spectra of the pristine hydrogel (Hgel-Norm), Fe-functionalized PANI–PA hydrogel (Hgel-Fe_{0.4}), and Co-functionalized PANI–PA hydrogel (Hgel-Co_{0.4}). The spectra show the peaks for (a) C 1s, (b) N 1s, (c) O 2p, (d) P 2p, (e) Fe 2p, and (f) Co 2p.

too small to see in these TEM images, as expected, because they are in the form of isolated ions bound to the polymer with coordination bonds, or not nanosized/in the crystalline form, as also indicated by XRD earlier.

N₂ adsorption–desorption is used to determine the surface areas of the materials (Figure S15). The Brunauer–Emmett–Teller specific surface area of the dehydrated pristine hydrogel is 38 m² g^{−1}, while those of Fe-functionalized and Co-functionalized hydrogels are 63 and 43 m² g^{−1}, respectively, and that of

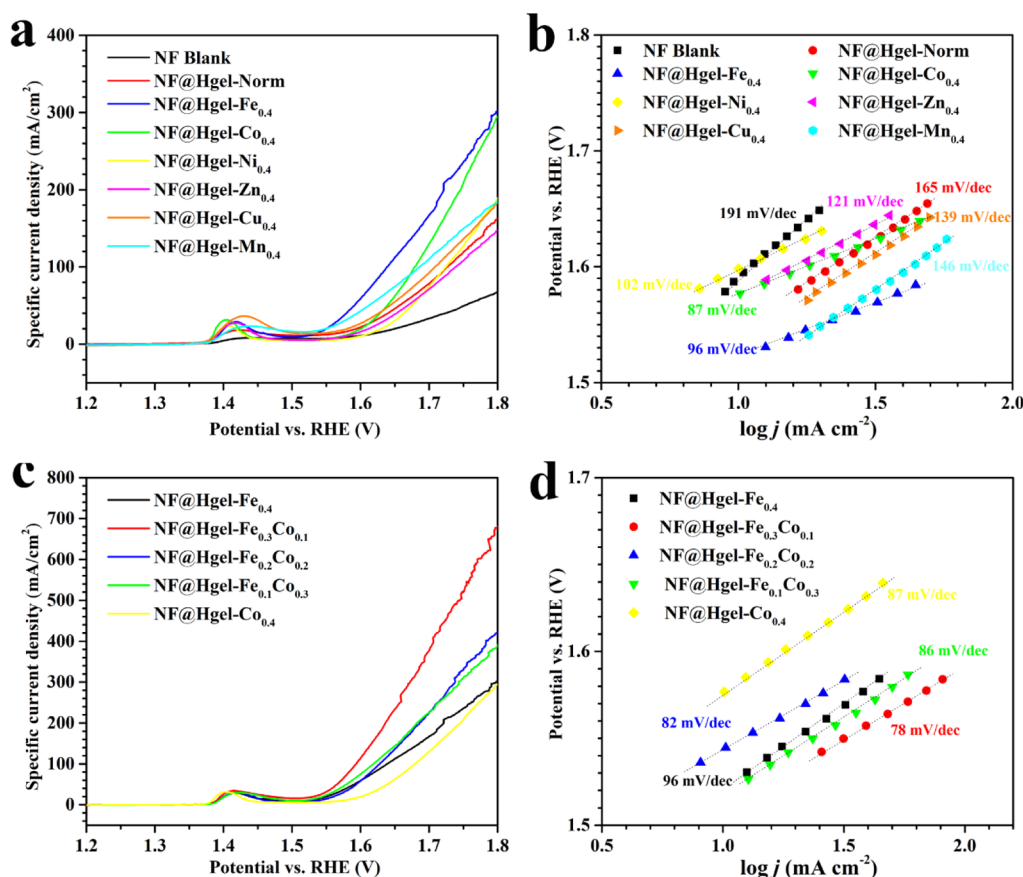


Figure 4. (a) Steady-state polarization curves and (b) Tafel plots for OER in a 1 M KOH solution over various NF-supported metal-functionalized hydrogels electrocatalysts and their corresponding control materials (NF@Hgel-Norm and NF Blank). (c) Steady-state polarization profiles and (d) Tafel plots of the OER in a 1 M KOH solution over different NF-supported Fe- and Co-functionalized hydrogels during OER.

Fe and Co cofunctionalized hydrogel is $57 \text{ m}^2 \text{ g}^{-1}$. These results indicate that including Fe and Co in the synthesis of the hydrogels creates higher surface areas in them. This is particularly true for Fe (compared with Co). This is not surprising though, given the fact that Fe is incorporated in the hydrogel more and alters the hydrogel's structure more prominently, as discussed earlier. Note also that Fe and Co cofunctionalized hydrogels possess a lot more Fe than Co, even in the case where the same amounts of both metals are used for the synthesis of the hydrogels (see the ICP-OES results presented in Table S1 in the Supporting Information).

XPS is performed to investigate the surface chemical composition of the hydrogels. The full survey XPS spectra of the materials (Figures S16–S18) show the presence of C, N, O, P, and Fe/Co. The high-resolution XPS spectrum of C 1s of the pristine hydrogel (Figure 3a) shows a peak at 284.6 eV corresponding to the C–C and C=C groups in PANI and PA, a peak at 286.3 eV corresponding to the carbon atoms in the C–N bonds in PANI chains, and a peak at 288.7 eV corresponding to the carbon atoms in C=O bonds in PA.⁸ After functionalization with Fe^{3+} ions, the peak corresponding to C–N groups in the hydrogel increases according to the amount of Fe^{3+} ions used to synthesize the hydrogels (Figures 3a and S17a). This could be because Fe promotes the polymerization of PANI, giving rise to more C–N groups.^{12,26} The reduction in the intensity of the C 1s peak of C=O in this material is due to the electron transfer from C=O to the metal as a result of the formation of Fe–O coordination bonds when the hydrogel is functionalized with Fe^{3+} ions.

The high-resolution XPS spectra of N 1s of all materials (Figures 3b and S17b) show peaks at 399.4 eV due to quinoid ($-\text{N}=\text{N}-$) and benzenoid ($-\text{NH}-$) groups and a peak at 402.3 eV due to quaternary ammonium (N^+) groups.²⁷ High-resolution XPS spectra of O 2p of the pristine hydrogel (Figures 3c and S17c) show peaks at 530.6 and 532.3 eV corresponding to O=C and O–P groups, respectively.²⁸ The spectrum of Fe-functionalized hydrogel also shows a peak at 532.1 eV associated with O 2p of O–Fe bonds in the hydrogel.^{29–31} In addition, the one for Co-functionalized hydrogel shows a peak at 532.9 eV due to O 2p in O–Co bonds in the hydrogel.³² The corresponding spectra of Fe- and Co-cofunctionalized hydrogels show similar peaks attributable to O–Fe/Co groups, which can form between the metals and the O atoms in PA. Meanwhile, all high-resolution spectra of P 2p reveal a peak in the range of 133–134 eV (see Figures 3d and S17d), which can be ascribed to the P–O species in PA.^{9,28,32} This peak is noticeably shifted from 133.66 to 134.03 eV as the amount of Fe in the hydrogel is increased, indicating a higher degree of electron transfer from P–O groups to Fe–OH species.³² XPS spectra of all Fe-functionalized hydrogels also show peaks at 712.8, 736.9, 725.2, and 729.8 eV that are due to Fe 2p of Fe^{3+} species (Figures 3e, S17e and S18b).^{29,30,33} However, the XPS spectra of all Co-cofunctionalized hydrogels (Figures 3f, S17f, and S18c) show very small peaks associated with Co 2p, further corroborating the low amount of Co present in them.

3.2. Electrocatalytic Properties of Hydrogels for OER.

Given their reasonably large surface area and nanoporous structures with abundant and well-distributed transition metals,

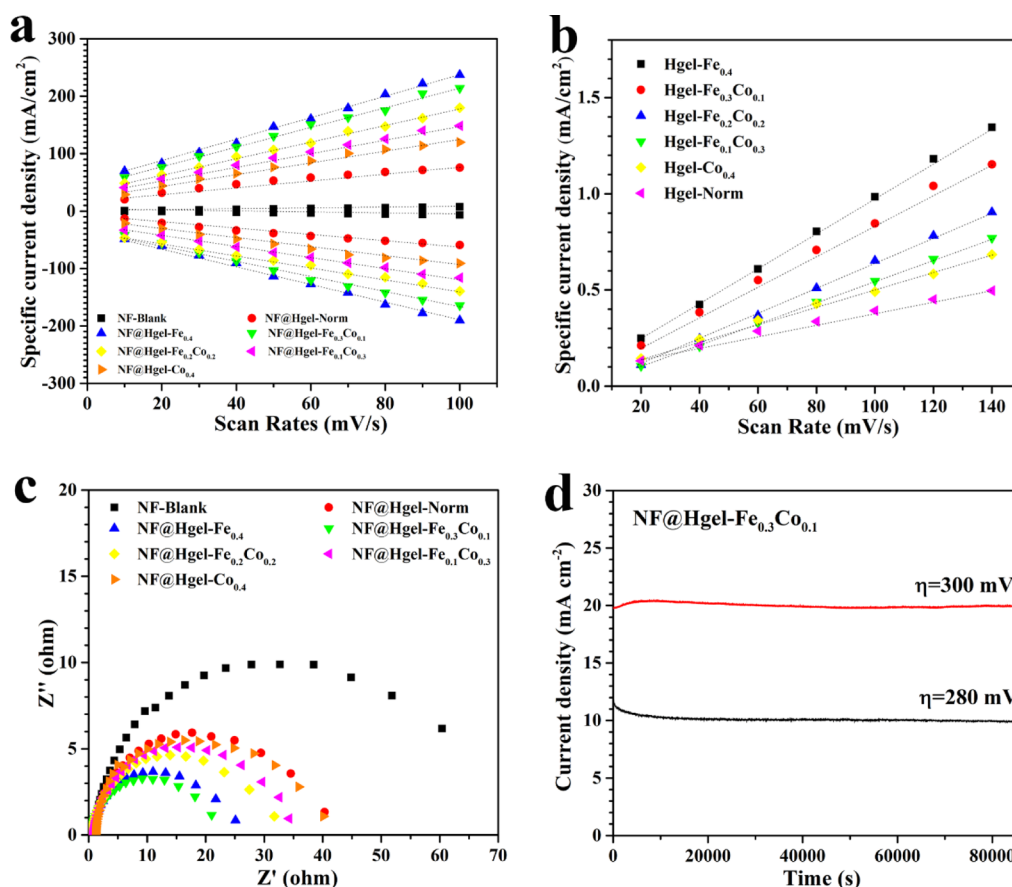
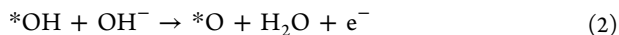


Figure 5. Plots of (a) anodic and cathodic peak current densities versus scan rate; (b) current density versus scan rate; and (c) EIS obtained at an overpotential of 350 mV for NF-Blank, NF@Hgel-Norm, NF@Hgel-Fe_{0.4}, NF@Hgel-Fe_{0.3}Co_{0.1}, NF@Hgel-Fe_{0.2}Co_{0.2}, NF@Hgel-Fe_{0.1}Co_{0.3}, and NF@Hgel-Co_{0.4}. (d) Current density versus time (*i*–*t*) plots for the OER in 1 M KOH solution over of NF@Hgel-Fe_{0.3}Co_{0.1} at overpotentials of 280 and 300 mV versus SCE for 24 h.

we expected that these metal-functionalized hydrogels electrocatalyze OER well. This has been found to be the case in alkaline solutions, as detailed below. The first step in OER entails the adsorption of OH[−] ions from the solution onto the active sites of the catalyst, to be followed by the transformation of the OH[−] ions into *OH species by releasing an electron, as shown in eq 1. (Note that the catalytic site of a solid catalyst is often represented by *).



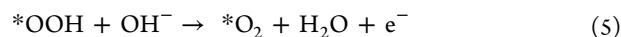
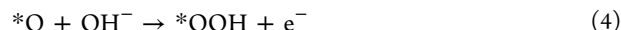
This elementary step is followed by a reaction between the *OH groups on the catalyst and OH[−] species present in the solution to form surface-adsorbed oxide (*O), H₂O, and an electron, as denoted in eq 2.



Then, one of the following two possible mechanisms ensues, depending on the catalyst. The first one, which is named Mechanism 1 herein, involves the combination of two *O adsorbates to produce O₂, as shown in eq 3.



The second one, which is denoted as Mechanism 2, involves three steps, namely, the hydroxylation of *O to form *OOH, then a reaction between *OOH and OH[−] to produce dioxygen on the surface of the catalyst (*O₂), and eventually the desorption of dioxygen from the catalyst's surface, as molecular O₂ (eqs 4–6).



Generally, by obtaining polarization curves, how the OER takes place over the surfaces of a given electrocatalyst (or the mechanism) and the activity of the catalyst can be determined. Thus, steady-state polarization studies of OER are carried out over the hydrogels by supporting them on NF. The results, compiled in Figure 4a,b and Table S3, show that Fe-functionalized and Co-functionalized hydrogels supported on NF need lower overpotentials or exhibit greater electrocatalytic activities for OER than all other hydrogels. When NF@Hgel-Fe_{0.4} and NF@Hgel-Co_{0.4} are compared with each other, the overpotential of the reaction over the former is lower than that of the latter. For example, the former requires 320 mV to drive the reaction at a current density of 20 mV cm^{−2} (*η*₂₀), whereas the latter requires 370 mV (or a higher potential) to do the same. Interestingly, the latter can drive the reaction with the same current density as the former when the potential reaches 1.8 V (or 1800 mV). Accordingly, the Tafel slope of the latter (which is found to be 87 mV dec^{−1}) is smaller than that of the former (whose Tafel slope is found to be 96 mV dec^{−1}). This means that the OER over NF@Hgel-Co_{0.4} has a slightly faster kinetics compared with the one over NF@Hgel-Fe_{0.4}, despite the latter's better onset potential.

Due to PANI–PA hydrogel's unique, high ability to accommodate Fe, hydrogels with different amounts of Fe could also be synthesized by varying the concentration of Fe ions used in the solution, and then studied (Figure S19). While adding more Fe into the hydrogel improves the hydrogel's electrocatalytic activity toward OER, excess Fe is not found to do so, though. In fact, interestingly, including rather a small amount of Co into the hydrogel along with Fe increases the electrocatalytic activity of the hydrogel further. Detailed results of the catalytic activities of Fe- and Co-cofunctionalized hydrogels containing different amounts of Fe and Co for OER are displayed in Figure 4c,d. Note that all Fe- and Co-cofunctionalized hydrogels show better electrocatalytic activities for OER compared with the other metal-functionalized hydrogels. NF@Hgel-Fe_{0.3}Co_{0.1} particularly shows the best electrocatalytic activity, by requiring overpotentials of only 280 and 300 mV to drive OER at current densities of 10 mV cm⁻² (η_{10}) and 20 mV cm⁻² (η_{20}), respectively. These values also render this hydrogel one of the best OER electrocatalysts reported to date (see Table S6). The material gives the lowest Tafel slope (78 mV dec⁻¹) as well, indicating the facile OER kinetics taking place on it. Furthermore, this Tafel slope indicates that the OER over this electrocatalyst proceeds through Mechanism 2 that is described earlier.

The electrochemical properties of Fe- and Co-cofunctionalized hydrogels are further investigated by determining the surface coverage of M(OH)₂/MOOH (M = Fe or Co) redox species and the electroactivity of PANI (Γ^*) in them. This is done using the CV curves obtained for them during OER at different scan rates and their anodic and cathodic currents (see Figures 5a and S20).³⁴ For comparison, the same measurements are carried out for NF@Hgel-Norm and NF-Blank. The results, compiled in Table S4, show that the value of Γ^* of NF@Hgel-Norm is 0.575×10^{-6} mol cm⁻², which is 7 times higher than that of NF-Blank (whose corresponding value is 0.772×10^{-7} mol cm⁻²). This shows PANI's great ability to undergo redox processes (or its electroactivity). The values of Γ^* of metal-functionalized hydrogels are even larger. For example, the value of Γ^* of NF@Hgel-Co_{0.4} is 0.960×10^{-6} mol cm⁻², which is 1.7 times higher than that of pristine hydrogel (NF@Hgel-Norm). This indicates that the Co atoms present in the hydrogels, albeit their small amount, improve the redox processes on the polymer in the hydrogel. The values of Γ^* of Fe-functionalized hydrogels are even higher, concomitant to the amount of Fe dopants in them. For example, the value of Γ^* of NF@Hgel-Fe_{0.4} is 1.879×10^{-6} mol cm⁻², which is 3.2-times higher than that of pristine hydrogel. Notably also, NF@Hgel-Fe_{0.4} has a considerably larger oxidation peak current density, indicating the existence of a large amount of surface redox species on it. This suggests that the Fe ions incorporated within the hydrogel transform into Fe(OH)₂/FeOOH species. Note that these hydroxide and oxyhydroxide species of Fe are well-known OER electrocatalysts.^{35,36} Furthermore, the redox species on NF@Hgel-Fe_{0.4} is substantially greater than those in many notable metallic electrocatalysts reported in the literature; for example, the redox species in this hydrogel is 4.8, 8.9, 15.7, and 21.1 times larger than that of Ni₉₇Bi₃ (3.9×10^{-7} mol cm⁻²),¹⁸ NiSn(2:1) (2.1×10^{-7} mol cm⁻²),³⁷ Ni_{0.5}Co_{0.5}Sn (1.2×10^{-8} mol cm⁻²),³⁸ and Ni–C-30 (8.9×10^{-8} mol cm⁻²).³⁹

Next, the electrochemical double-layer capacitance (C_{dl}), which is directly correlated to the electrochemical active surface area, of the materials are determined and compared among one another (Figures 5b and S21 and Table S5). All hydrogels have

high values of C_{dl} , especially compared with that of blank NF, partly due to their interconnected porous nanostructures. This means, the electrocatalytic active sites in the hydrogels are accessible for OER. Interestingly, the values of C_{dl} of Fe-functionalized hydrogel increase as the amount of Fe used in them increases (Table S5). This means the Fe used during the synthesis of the hydrogel, which produces an increased surface area, creates more surface-exposed, electrochemically active sites in the hydrogel for OER. The values of C_{dl} of metal-functionalized hydrogels also generally increase as the amounts hydrogels on NF are increased.

The high electrocatalytic activity of metal-functionalized hydrogels for OER is also associated with the hierarchical 3D conductive PANI–PA structure, which enables a fast charge transfer during the reaction. This is evidenced based on the EIS of the hydrogels obtained at an overpotential of 350 mV (Figure 5c). Compared with the charge-transfer resistance (R_{ct}) of NF-Blank, which is 69 Ω , that of NF@Hgel-Norm ($R_{ct} = 43 \Omega$) is much lower. Notably also, the Fe-functionalized hydrogels display even smaller values of R_{ct} , with the values being dependent on the amounts of Fe in them (e.g., the values for NF@Hgel-Fe_{0.4}, NF@Hgel-Fe_{0.3}Co_{0.1}, NF@Hgel-Fe_{0.2}Co_{0.2}, and NF@Hgel-Fe_{0.1}Co_{0.3} are 26, 23, 34, and 36 Ω , respectively). This also highlights the importance of Fe in creating fast charge-transfer properties in these hydrogels. Overall, the conductivity of the PANI–PA network can markedly facilitate charge transfer during electrocatalytic OER, while its porous and hydrophilic surfaces produce good contact between the polymer and the underlying substrate as well as a good transport pathways for electrolytes through the hydrogel.

Based on the above results, the high electrocatalytic activity of NF@Hgel-Fe_{0.3}Co_{0.1} for OER can be attributed to the following three factors. (1) The partially positively charged carbon atoms on phytate/PA groups in the PANI–PA hydrogel could serve as active catalytic sites for OER, as their parent compound, PA, has been previously reported to electrocatalyze OER.⁸ (2) The high ESCA of the metal-functionalized hydrogels, which is partly due to the metal dopants, can assist with electrocatalysis. (3) The metallic species incorporated into the hydrogels provide P–O–M groups, where M is Fe or Co, and these groups could serve as catalytic sites for OER.^{40,41} Note that the presence of P–O–Co and P–O–Fe groups has been evidenced based on the XPS spectra of NF@Hgel-Co_{0.4} and NF@Hgel-Fe_{0.4}, respectively. Note also that P–O–Co groups were previously reported to electrocatalyze OER with a low Tafel slope than the P–O–Fe groups.^{40,41} These metallic groups also promote the breakage of the OH bond and assist with the formation of the O–O bond by tuning the energies associated with the reaction intermediates (*OH, *O, and *OOH). The adsorption of these three species is stronger on the Fe site than at the Co site.^{40,42} Previous reports also indicated that the adsorption energy of H₂O on P–Fe/Co is much lower than that on P–Co.⁴³ Thus, P–Fe–Co groups show a better electrocatalytic activity than P–Fe or P–Co groups.^{44,45} Additionally, the copresence of Fe and Co atoms on the Fe- and Co-cofunctionalized hydrogels, as seen in their EDS-based elemental mapping images, could create adjacent bimetallic sites that can effectively electrocatalyze the reaction via synergistic effects.^{24,46,47}

As polymer-based electrocatalysts with porous structures and hydrophilic surfaces, these hydrogels can be expected to form a good contact between their catalytic sites and an electrode. They can also be easily spray-coated on the surfaces of various electrodes to form electrocatalysts with good mass transport and

reaction kinetics. As a result, they can be more suitable than conventional powder-based catalysts for practical use. By taking these into consideration, a simple soak-and-dry method is adopted to load these polymer hydrogels onto the surface of the NF and carbon cloth (CC) in different loadings to study their performances in practical electrodes (Figures S22 and 23). Contact angle measurements for the Hgel-Fe_{0.3}Co_{0.1} catalyst and Hgel-Norm (the reference material) showed that they are both quite hydrophilic. As can be seen in Figure S22, the drops of water placed on them quickly get sucked in, indicating the strong hydrophilicity of these hydrogel materials.

The resulting electrodes also show electrocatalytic activity toward OER, and their activity depends on the amounts of hydrogels present on the electrodes. Those with less amount show inferior activity, which may be due to the partial coverage of NF or CC with the hydrogel materials. On the other hand, those with excess amounts of hydrogels do not lead to any further increase in catalytic activity, which may be due to the increase in charge-transfer resistance as a result of the increased thickness of the hydrogel layer on the substrates.^{48,49} Ultimately, the optimal loadings that give rise to the maximum activity are determined for both NF@Hgel-Fe_{0.3}Co_{0.1} and pristine hydrogel (Hgel-Norm) (Figures S23 and S24). The value of C_{dl} of both hydrogels loaded on NF cease to increase when the amounts of the hydrogels exceed a certain amount (see Figures S23 and S24). Based on the results, a coverage of 1.0 mg cm⁻² of NF@Hgel-Fe_{0.3}Co_{0.1} on NF and a coverage of 0.4 mg cm⁻² of NF@Hgel-Fe_{0.3}Co_{0.1} on CC are found to be optimal loadings for this hydrogel (i.e., the best performing one for electrocatalysis, as discussed earlier) on NF or CC substrates to produce maximum electrocatalytic activities toward OER for practical applications.

Finally, the long-term stability of the electrocatalysts during OER, which is another factor that governs their practical use, is determined. This is done by measuring the stability of NF@Hgel-Fe_{0.3}Co_{0.1} by chronoamperometry at an overpotential of 280 and 300 mV (Figure 5d). After 24 h of continuous operation in OER, the current density of NF@Hgel-Fe_{0.3}Co_{0.1} remains almost unchanged, signifying the outstanding stability of NF@Hgel-Fe_{0.3}Co_{0.1} during the reaction. This is also true for the hydrogels on the NF and CC substrates, as can be seen from their SEM images and XPS spectra (see S25–29). The comparative SEM images of blank NF versus those of pristine hydrogel and Hgel-Fe_{0.3}Co_{0.1} loaded on NF with simple soak-and-dry method (Figures S25–S27) indicate that both hydrogels are well dispersible on the surfaces of NF. Furthermore, after OER for 1 h, the morphologies of the hydrogels barely change, suggesting their stability on the electrodes during electrocatalysis.

To investigate their composition after the reaction, the materials are also characterized by XPS (see Figures S27 and S28). Their C 1s XPS spectra show peaks at 295 and 292.5 eV, which can be ascribed to the 2p_{1/2} and 2p_{3/2} electrons, respectively, of surface K atoms introduced onto the materials from the KOH solution that is used as an electrolyte.³⁶ The XPS spectra of N 1s show an obvious peak shift by 1.4 eV after OER, indicating that the –NH– groups in PANI are oxidized to=N– groups during OER.³⁷ All XPS spectra of O 2p show a stronger peak at 530.8 eV, which must be due to the formation of M(OOH) groups, where M represents the metals, that is, Fe, Co, or Ni, on the substrate.³⁸ These results imply that, during OER, the Fe and Co atoms in the hydrogels transform into Fe(OOH) and Co(OOH), which are highly active electrocatalysts for OER.³⁹

4. CONCLUSIONS

PANI–PA-based conducting hydrogels containing transition metals (Fe and/or Co) were synthesized, and their electrocatalytic activities for OER were demonstrated. The metals could be introduced into the hydrogel by taking advantage of the ability of the PA groups in the hydrogel to form coordination bonds with them. Among many transition metals investigated, Fe has been found to be taken up by the hydrogel at a much greater extent. These metal-immobilized hydrogels generally showed better electrocatalytic activities than the pristine hydrogel. In particular, the hydrogels functionalized with both Fe and Co have shown the highest electrocatalytic activity for OER. Among them, NF@Hgel-Fe_{0.3}Co_{0.1} has been found the most efficient to electrocatalyze OER with a current density of 10 mV cm⁻² in a 1 M KOH solution with an overpotential of only 280 mV. The hydrogels could also form a high density of redox species on their surfaces. By taking advantage of their processability, the hydrogels could easily be loaded onto NF and CC substrates via a simple soak-and-dry method and form free-standing electrodes for OER. The work could thus provide a new direction for the development of other conductive polymer hydrogels with heterogenized transition metals, or sustainable electrocatalysts, for OER and other renewable energy applications.

■ ASSOCIATED CONTENT

Supporting Information

The Supporting Information is available free of charge at <https://pubs.acs.org/doi/10.1021/acsami.2c01667>.

Results and discussion, including a digital synthetic procedure, XRD patterns, TGA curves, ICP-OES analysis results, Raman spectra, FTIR spectra, UV–vis absorption spectra, SEM, TEM, and EDS mapping images, nitrogen (N₂) adsorption–desorption isotherms, XPS spectra, LSV curves, summary of electrochemical performances, CV curves about capacitance and redox species, contact angle images for hydrophilicity, LSV curves about catalyst loading, comparison of summarized references, and comparison SEM images of the pristine hydrogel, metal-functionalized hydrogels, blank NF, and hydrogel-loaded NFs (PDF)

■ AUTHOR INFORMATION

Corresponding Author

Tewodros Asefa – Department of Chemistry and Chemical Biology, Rutgers, The State University of New Jersey, Piscataway, New Jersey 08854, United States; Department of Chemical and Biochemical Engineering, Rutgers, The State University of New Jersey, Piscataway, New Jersey 08854, United States; orcid.org/0000-0001-8634-5437; Email: tasefa@chem.rutgers.edu

Authors

Chaoyun Tang – Hoffmann Institute of Advanced Materials, Shenzhen Polytechnic, Shenzhen 518060, China; Department of Chemistry and Chemical Biology, Rutgers, The State University of New Jersey, Piscataway, New Jersey 08854, United States; Department of Chemical and Biochemical Engineering, Rutgers, The State University of New Jersey, Piscataway, New Jersey 08854, United States

Belvin Thomas – Department of Chemistry and Chemical Biology, Rutgers, The State University of New Jersey, Piscataway, New Jersey 08854, United States

Maricely Ramírez-Hernández – Department of Chemical and Biochemical Engineering, Rutgers, The State University of New Jersey, Piscataway, New Jersey 08854, United States

Eliška M. Mikmeková – Department of Chemistry and Chemical Biology, Rutgers, The State University of New Jersey, Piscataway, New Jersey 08854, United States; Institute of Scientific Instruments, Czech Academy of Sciences, Brno 612 64, Czech Republic

Complete contact information is available at:
<https://pubs.acs.org/10.1021/acsami.2c01667>

Notes

The authors declare no competing financial interest.

ACKNOWLEDGMENTS

C.T. acknowledges the financial support from Post-doctoral Later-stage Foundation Project of Shenzhen Polytechnic (6019211006K).

REFERENCES

- (1) Wang, J.; Cui, W.; Liu, Q.; Xing, Z.; Asiri, A. M.; Sun, X. Recent Progress in Cobalt-based Heterogeneous Catalysts for Electrochemical Water Splitting. *Adv. Mater.* **2016**, *28*, 215–230.
- (2) Jia, Y.; Zhang, L.; Gao, G.; Chen, H.; Wang, B.; Zhou, J.; Soo, M. T.; Hong, M.; Yan, X.; Qian, G.; Zou, J.; Du, A.; Yao, X. A Heterostructure Coupling of Exfoliated Ni-Fe Hydroxide Nanosheet and Defective Graphene as a Bifunctional Electrocatalyst for Overall Water Splitting. *Adv. Mater.* **2017**, *29*, 1700017.
- (3) Tahir, M.; Pan, L.; Idrees, F.; Zhang, X.; Wang, L.; Zou, J.-J.; Wang, Z. L. Electrocatalytic Oxygen Evolution Reaction for Energy Conversion and Storage: A Comprehensive Review. *Nano Energy* **2017**, *37*, 136–157.
- (4) Fu, S.; Zhu, C.; Song, J.; Engelhard, M. H.; Li, X.; Du, D.; Lin, Y. Highly Ordered Mesoporous Bimetallic Phosphides as Efficient Oxygen Evolution Electrocatalysts. *ACS Energy Lett.* **2016**, *1*, 792–796.
- (5) Gong, M.; Dai, H. A Mini Review of NiFe-based Materials as Highly Active Oxygen Evolution Reaction Electrocatalysts. *Nano Res* **2015**, *8*, 23–39.
- (6) Zhang, B.; Zheng, X.; Voznyy, O.; Comin, R.; Bajdich, M.; García-Melchor, M.; Han, L.; Xu, J.; Liu, M.; Zheng, L.; García de Arquer, F. P.; Dinh, C. T.; Fan, F.; Yuan, M.; Yassitepe, E.; Chen, N.; Regier, T.; Liu, P.; Li, Y.; De Luna, P.; Janmohamed, A.; Xin, H. L.; Yang, H.; Vojvodic, A.; Sargent, E. H. Homogeneously Dispersed Multimetal Oxygen-evolving Catalysts. *Science* **2016**, *352*, 333–337.
- (7) Pan, L.; Yu, G.; Zhai, D.; Lee, H. R.; Zhao, W.; Liu, N.; Wang, H.; Tee, B. C.-K.; Shi, Y.; Cui, Y.; Bao, Z. Hierarchical Nanostructured Conducting Polymer Hydrogel with High Electrochemical Activity. *Proc. Natl. Acad. Sci. U.S.A.* **2012**, *109*, 9287–9292.
- (8) Hu, Q.; Li, G.; Liu, X.; Zhu, B.; Chai, X.; Zhang, Q.; Liu, J.; He, C. Superhydrophilic Phytic-Acid-Doped Conductive Hydrogels as Metal-Free and Binder-Free Electrocatalysts for Efficient Water Oxidation. *Angew., Chem. Int. Ed.* **2019**, *58*, 4318–4322.
- (9) Zhang, J.; Zhao, Z.; Xia, Z.; Dai, L. A Metal-Free Bifunctional Electrocatalyst for Oxygen Reduction and Oxygen Evolution Reactions. *Nat. Nanotechnol.* **2015**, *10*, 444–452.
- (10) Nielsen, A.; Tetens, I.; Meyer, A. Potential of Phytase-mediated Iron Release from Cereal-based Foods: A Quantitative View. *Nutrients* **2013**, *5*, 3074–3098.
- (11) Yu, S.; Cowieson, A.; Gilbert, C.; Plumstead, P.; Dalsgaard, S. Interactions of phytate and myo-inositol phosphate esters (IP1-5) including IP5 isomers with dietary protein and iron and inhibition of pepsin1. *J. Anim. Sci.* **2012**, *90*, 1824–1832.
- (12) Guo, Y.; Bae, J.; Fang, Z.; Li, P.; Zhao, F.; Yu, G. Hydrogels and Hydrogel-derived Materials for Energy and Water Sustainability. *Chem. Rev.* **2020**, *120*, 7642–7707.
- (13) A. Gabal, M.; Hussein, M.; Hermas, A. Synthesis, Characterization and Electrical Conductivity of Polyaniline-Mn_{0.8}Zn_{0.2}Fe₂O₄ Nano-composites. *Int. J. Electrochem. Sci.* **2016**, *11*, 4526–4538.
- (14) Atiqah, T. N.; Tan, S. J.; Foo, K. L.; Supri, A. G.; Al Bakri, A. M. M.; Liew, Y. M. Effect of Graphite Loading on Properties of Polyaniline/graphite Composites. *Polym. Bull.* **2018**, *75*, 209–220.
- (15) Kundu, S.; Satpati, B.; Kar, T.; Pradhan, S. Microstructure characterization of hydrothermally synthesized PANI/V₂O₅-nH₂O heterojunction photocatalyst for visible light induced photodegradation of organic pollutants and non-absorbing colorless molecules. *J. Hazard. Mater.* **2017**, *339*, 161–173.
- (16) Leng, C.; Wei, J.; Liu, Z.; Shi, J. Influence of imidazolium-based ionic liquids on the performance of polyaniline-CoFe₂O₄ nano-composites. *J. Alloys Compd.* **2011**, *509*, 3052–3056.
- (17) Zhang, Y.; Dou, C.; Li, L.; Wang, Y. A Practical Way to Prepare Thin Polyaniline Nanofibers with Ferric Nitrate as an Oxidant. *Polym. Sci., Ser. A* **2014**, *56*, 146–151.
- (18) Wang, H.; Lin, J.; Shen, Z. X. Polyaniline (Pani) Based Electrode Materials for Energy Storage and Conversion. *J. Sci.: Adv. Mater. Devices* **2016**, *1*, 225–255.
- (19) Yan, H.; Kajita, M.; Toshima, N. Polymerization of Aniline Using Iron(III) Catalyst and Ozone, and Kinetics of Oxidation Reactions in the Catalytic System. *Macromol. Mater. Eng.* **2002**, *287*, 503–508.
- (20) Moravkova, Z.; Trchová, M.; Tomsík, E.; Stejskal, J. Influence of Ethanol on the Chain-ordering of Carbonised Polyaniline. *Chem. Pap.* **2013**, *67*, 919–932.
- (21) Li, P.; Jin, Z.; Peng, L.; Zhao, F.; Xiao, D.; Jin, Y.; Yu, G. Stretchable All-Gel-State Fiber-Shaped Supercapacitors Enabled by Macromolecularly Interconnected 3D Graphene/Nanostructured Conductive Polymer Hydrogels. *Adv. Mater.* **2018**, *30*, 1800124.
- (22) Awata, R.; Shehab, M.; El Tahan, A.; Soliman, M.; Ebrahim, S. High Performance Supercapacitor Based on Camphor Sulfonic Acid Doped Polyaniline/multiwall Carbon Nanotubes Nanocomposite. *Electrochim. Acta* **2020**, *347*, 136229.
- (23) Bera, A.; Deb, K.; Kathirvel, V.; Bera, T.; Thapa, R.; Saha, B. Flexible Diode of Polyaniline/ito Heterojunction on Pet Substrate. *Appl. Surf. Sci.* **2017**, *418*, 264–269.
- (24) Tang, C.; Asefa, T. Ternary ZIF-8-derived dual-metal CoCu nanoparticles in porous carbon polyhedra as efficient catalysts for methanol oxidation. *J. Mater. Chem. A* **2020**, *8*, 12285–12290.
- (25) Kuang, M.; Han, P.; Wang, Q.; Li, J.; Zheng, G. CuCo Hybrid Oxides as Bifunctional Electrocatalyst for Efficient Water Splitting. *Funct. Mater.* **2016**, *26*, 8555–8561.
- (26) Mu, B.; Tang, J.; Zhang, L.; Wang, A. Facile fabrication of superparamagnetic graphene/polyaniline/Fe₃O₄ nanocomposites for fast magnetic separation and efficient removal of dye. *Sci. Rep.* **2017**, *7*, 5347.
- (27) Patil, S. H.; Gaikwad, A. P.; Sathaye, S. D.; Patil, K. R. To Form Layer by Layer Composite Film in View of Its Application as Supercapacitor Electrode by Exploiting the Techniques of Thin Films Formation Just around the Corner. *Electrochim. Acta* **2018**, *265*, 556–568.
- (28) Sun, X.; Brückner, C.; Lei, Y. One-pot and Ultrafast Synthesis of Nitrogen and Phosphorus Co-doped Carbon Dots Possessing Bright Dual Wavelength Fluorescence Emission. *Nanoscale* **2015**, *7*, 17278–17282.
- (29) Yang, H.; Shi, B.; Wang, S. Fe Oxides Loaded on Carbon Cloth by Hydrothermal Process as an Effective and Reusable Heterogeneous Fenton Catalyst. *Catalysts* **2018**, *8*, 207.
- (30) Yang, T.; Meng, L.; Han, S.; Hou, J.; Wang, S.; Wang, X. Simultaneous reductive and sorptive removal of Cr(VI) by activated carbon supported β -FeOOH. *RSC Adv* **2017**, *7*, 34687–34693.
- (31) Chen, X.; Zeng, Y.; Chen, Z.; Wang, S.; Xin, C.; Wang, L.; Shi, C.; Lu, L.; Zhang, C. Synthesis and Electrochemical Property of FeOOH/graphene Oxide Composites. *Front. Chem.* **2020**, *8*, 328.

- (32) Wang, S.; Nam, G.; Li, P.; Jang, H.; Wang, J.; Kim, M. G.; Wu, Z.; Liu, X.; Cho, J. Highly Active Bifunctional Oxygen Electrocatalysts Derived from Nickel- or Cobalt-phytic Acid Xerogel for Zinc-air Batteries. *Nanoscale* **2018**, *10*, 15834–15841.
- (33) Wang, T.; Jiang, Z.; Chu, K. H.; Wu, D.; Wang, B.; Sun, H.; Yip, H. Y.; An, T.; Zhao, H.; Wong, P. K. X-Shaped α -FeOOH with Enhanced Charge Separation for Visible-Light-Driven Photocatalytic Overall Water Splitting. *ChemSusChem* **2018**, *11*, 1365–1373.
- (34) Dubale, A. A.; Zheng, Y.; Wang, H.; Hübner, R.; Li, Y.; Yang, J.; Zhang, J.; Sethi, N. K.; He, L.; Zheng, Z.; Liu, W. High-Performance Bismuth-Doped Nickel Aerogel Electrocatalyst for the Methanol Oxidation Reaction. *Angew., Chem. Int. Ed.* **2020**, *59*, 13891–13899.
- (35) Liu, S.; Zhang, J.; Wang, H.; Asefa, T.; Huang, X. A Facile Route to Efficient Water Oxidation Electrodes Via Electrochemical Activation of Iron in Nickel Sulfate Solution. *ACS Sustainable Chem. Eng.* **2020**, *8*, 15550–15559.
- (36) Danilovic, N.; Subbaraman, R.; Strmcnik, D.; Chang, K.-C.; Paulikas, A. P.; Stamenkovic, V. R.; Markovic, N. M. Enhancing the Alkaline Hydrogen Evolution Reaction Activity through the Bifunctionality of Ni(OH)₂/Metal Catalysts. *Angew., Chem. Int. Ed.* **2012**, *51*, 12495–12498.
- (37) Li, J.; Luo, Z.; Zuo, Y.; Liu, J.; Zhang, T.; Tang, P.; Arbiol, J.; Llorca, J.; Cabot, A. Nisn Bimetallic Nanoparticles as Stable Electrocatalysts for Methanol Oxidation Reaction. *Appl. Catal., B* **2018**, *234*, 10–18.
- (38) Li, J.; Luo, Z.; He, F.; Zuo, Y.; Zhang, C.; Liu, J.; Yu, X.; Du, R.; Zhang, T.; Infante-Carrió, M. F.; Tang, P.; Arbiol, J.; Llorca, J.; Cabot, A. Colloidal Ni-Co-Sn nanoparticles as efficient electrocatalysts for the methanol oxidation reaction. *J. Mater. Chem. A* **2018**, *6*, 22915–22924.
- (39) Zhang, S.-J.; Zheng, Y.-X.; Yuan, L.-S.; Zhao, L.-H. Ni-B amorphous alloy nanoparticles modified nanoporous Cu toward ethanol oxidation in alkaline medium. *J. Power Sources* **2014**, *247*, 428–436.
- (40) Liu, K.; Zhang, C.; Sun, Y.; Zhang, G.; Shen, X.; Zou, F.; Zhang, H.; Wu, Z.; Wegener, E. C.; Taubert, C. J.; Miller, J. T.; Peng, Z.; Zhu, Y. High-performance Transition Metal Phosphide Alloy Catalyst for Oxygen Evolution Reaction. *ACS Nano* **2018**, *12*, 158–167.
- (41) Han, X.; Yu, C.; Zhou, S.; Zhao, C.; Huang, H.; Yang, J.; Liu, Z.; Zhao, J.; Qiu, J. Ultrasensitive Iron-Triggered Nanosized Fe-CoOOH Integrated with Graphene for Highly Efficient Oxygen Evolution. *Adv. Energy Mater.* **2017**, *7*, 1602148.
- (42) Tan, Y.; Wang, H.; Liu, P.; Shen, Y.; Cheng, C.; Hirata, A.; Fujita, T.; Tang, Z.; Chen, M. Versatile Nanoporous Bimetallic Phosphides Towards Electrochemical Water Splitting. *Energy Environ. Sci.* **2016**, *9*, 2257–2261.
- (43) Zhou, L.; Shao, M.; Li, J.; Jiang, S.; Wei, M.; Duan, X. Two-dimensional Ultrathin Arrays of CoP: Electronic Modulation toward High Performance Overall Water Splitting. *Nano Energy* **2017**, *41*, 583–590.
- (44) Wang, Y.; Liu, D.; Liu, Z.; Xie, C.; Huo, J.; Wang, S. Porous cobalt-iron nitride nanowires as excellent bifunctional electrocatalysts for overall water splitting. *Chem. Commun.* **2016**, *52*, 12614–12617.
- (45) Mendoza-Garcia, A.; Su, D.; Sun, S. Sea urchin-like cobalt-iron phosphide as an active catalyst for oxygen evolution reaction. *Nanoscale* **2016**, *8*, 3244–3247.
- (46) Han, L.; Dong, S.; Wang, E. Transition-metal (Co, Ni, and Fe)-based Electrocatalysts for the Water Oxidation Reaction. *Adv. Mater.* **2016**, *28*, 9266–9291.
- (47) Wang, X.; Yu, L.; Guan, B. Y.; Song, S.; Lou, X. W. D. Metal-Organic Framework Hybrid-Assisted Formation of Co₃O₄/Co-Fe Oxide Double-Shelled Nanoboxes for Enhanced Oxygen Evolution. *Adv. Mater.* **2018**, *30*, 1801211.
- (48) Hua, M.; Wu, S.; Jin, Y.; Zhao, Y.; Yao, B.; He, X. Tough-Hydrogel Reinforced Low-Tortuosity Conductive Networks for Stretchable and High-Performance Supercapacitors. *Adv. Mater.* **2021**, *33*, 2100983.
- (49) Pan, S.; Zhang, F.; Cai, P.; Wang, M.; He, K.; Luo, Y.; Li, Z.; Chen, G.; Ji, S.; Liu, Z.; Loh, X. J.; Chen, X. Mechanically Interlocked

Hydrogel-Elastomer Hybrids for On-Skin Electronics. *Adv. Funct. Mater.* **2020**, *30*, 1909540.